EDGE ARTICLE

Check for updates

Metal–organic frameworks as hypergolic additives for hybrid rockets†

Olivier Jobin, [ID] [a] Cristina Mottillo,[b] Hatem M. Titi, [ID] [c] Joseph M. Marrett,[c] Mihails Arhangelskis,[d] Robin D. Rogers,*[e] Bachar Elzein,[f] Tomislav Friščić [ID] *[c] and Étienne Robert [ID] *[a]

Hybrid rocket propulsion can contribute to reduce launch costs by simplifying engine design and operation. Hypergolic propellants, *i.e.* igniting spontaneously and immediately upon contact between fuel and oxidizer, further simplify system integration by removing the need for an ignition system. Such hybrid engines could also replace currently popular hypergolic propulsion approaches based on extremely toxic and carcinogenic hydrazines. Here we present the first demonstration for the use of hypergolic metal–organic frameworks (HMOFs) as additives to trigger hypergolic ignition in conventional paraffin-based hybrid engine fuels. HMOFS are a recently introduced class of stable and safe hypergolic materials, used here as a platform to bring readily tunable ignition and combustion properties to hydrocarbon fuels. We present an experimental investigation of the ignition delay (ID, the time from first contact with an oxidizer to ignition) of blends of HMOFs with paraffin, using White Fuming Nitric Acid (WFNA) as the oxidizer. The majority of measured IDs are under 10 ms, significantly below the upper limit of 50 ms required for functional hypergolic propellant, and within the ultrafast ignition range. A theoretical analysis of the performance of HMOFs-containing fuels in a hybrid launcher engine scenario also reveals the effect of the HMOF mass fraction on the specific impulse (I_{sp}) and density impulse (ρI_{sp}). The use of HMOFs to produce paraffin-based hypergolic fuels results in a slight decrease of the I_{sp} and ρI_{sp} compared to that of pure paraffin, similar to the effect observed with Ammonia Borane (AB), a popular hypergolic additive. HMOFs however have a much higher thermal stability, allowing for convenient mixing with hot liquid paraffin, making the manufacturing processes simpler and safer compared to other hypergolic additives such as AB.

1 Introduction

For small space technology companies, designing engines based on well established, albeit reliable, propellants is not always an attractive option, either due to their high toxicity, or requirements for complex engine designs. For example, hydrazine and its derivatives monomethylhydrazine (MMH) and unsymmetrical dimethylhydrazine (UDMH)[1] have been used for

over 60 years as both satellite and rocket fuels due to their reliable combustion properties. However, their extreme toxicity and difficult handling represent significant challenges and have motivated a future ban for the use of these propellants in the European Union.[2] Other propellants systems, using liquid oxygen as the oxidizer and hydrogen or RP-1 as the fuel, are less toxic or non-toxic, but still require costly storage techniques and involve complex liquid-fueled cryogenic engines.[3] The cost of developing and using engines based on such propellants is an obstacle for the companies aiming to democratize access to space and serve the burgeoning microsatellite industry. The desire to mitigate the impact of this emergent space industry on the environment, while making launches simpler, safer and less costly, calls for the development of innovative solutions to propulsion challenges adapted to small-scale launchers.[4] Recently developed propulsion approaches such as ion thrusters,[5] water-splitting,[6] and solar-powered engines[7] are simpler and safer than chemical propulsion, but are not suitable for all applications. For instance, ground-to-orbit missions as well as rapid-response spacecraft orbital manoeuvring and attitude correction require high thrust that these novel

[a]Department of Mechanical Engineering, Polytechnique Montréal, 2900 Boulevard Edouard-Montpetit, Montréal, QC H3T 1J4, Canada. E-mail: etienne.robert@polymtl.ca

[b]ACSYNAM Inc., Montréal, QC H1P 1W1, Canada

[c]Department of Chemistry, McGill University, 801 Sherbrooke Street West, Montréal, QC H2L 0B7, Canada. E-mail: tomislav.friscic@mcgill.ca

[d]University of Warsaw, 1 Pasteura Street, Warsaw, 02-093, Poland

[e]525 Solutions, P.O. Box 2206, Tuscaloosa, Al 35403, USA. E-mail: robin.rogers@525solutions.com

[f]Reaction Dynamics, 45 Chemin de l'Aéroport, Saint-Jean-sur-Richelieu, QC J3B 7B5, Canada

† Electronic supplementary information (ESI) available. See DOI: 10.1039/d1sc05975k

Table 1 Theoretical maximum I_{sp} values for common propellants[1]

Fuel/oxidizer	I_{sp} [s]	Type of engines
LO$_x$/Liquid hydrogen (LH$_2$)	386	Liquid
N$_2$O$_4$/UDMH	278	Liquid, hypergolic
RP-1/O$_2$	285	Liquid
HTPB-AP-Al	260–265	Solid
AMF-M315E	231–248 (ref. 30)	Monopropellant, hypergolic
SHP163	276 (ref. 31)	Monopropellant, hypergolic

propulsion approaches cannot provide (*e.g.* the International Space Station carries *ca.* 1 ton of hypergolic hydrazines[8]). Consequently, chemical propulsion is still the choice for rocket launchers or in-orbit maneuvering,[9,10] with hybrid engines an attractive alternative to complex, and therefore more costly, liquid-fueled engines.[11] To replace polluting propellants and enable competitive small-scale launchers, new technologies[12–29] should match or exceed the performance metrics of currently used propulsion approaches. For instance, the characteristic velocity (C^*) is a measure of the combustion performance of a rocket propulsion system, independent of its nozzle. The typical C^* value for liquid oxygen and RP-1 is approximately 1774 m s^{-1} at an optimal oxidizer-to-fuel ratio (O/F) of 2.24, while it is of 1711 m s^{-1} for the hypergolic, but highly toxic, combination of dinitrogen tetroxide (N$_2$O$_4$) and a mixture of 50% UDMH with 50% hydrazine at an O/F of 2.00.[1] Another important performance metric is the specific impulse (I_{sp}), which is the change in velocity per unit of propellant consumed. Typical I_{sp} values for commonly used propellant mixtures for liquid and solid engines are listed in Table 1. The cryogenically stored propellant mixture of liquid oxygen (LO$_x$) and liquid hydrogen (LH$_2$) has a theoretical I_{sp} of 386 s, which is generally considered to be the upper limit in chemical propulsion.[1] For comparison, solid rocket boosters (SRBs), the simplest rocket propulsion approach, can provide I_{sp} values of approximately 260–265 s when mixtures of hydroxyl-terminated polybutadiene (HTPB), aluminum powder (Al) and the oxidizer ammonium perchlorate (AP) are used.[1,30,31] These values are comparable to hypergolic hydrazine fuels, but the thrust of SRBs cannot be stopped nor throttled.

To fulfill its potential of reduced development costs and improving mechanical simplicity, hybrid rocket propulsion is in need of novel propellant systems to be competitive for launch vehicle applications, especially regarding specific and density impulses. This can be achieved with energy-dense additives in fuel grains made of solid hydrocarbons, including metal or organic hydrides and crystalline metals.[32,33] As an example, the incorporation of aluminum particles has been shown to improve the specific impulse of hybrid propellants relying on relatively weak oxidizers such as hydrogen peroxide or nitrous oxide.[32] Another way of making hybrid rockets more interesting is by inducing the hypergolic ignition of its fuel. Additives such as ammonia borane (AB) can be included in a fuel matrix.[25,29,33,34] On contact with the oxidizer, white fuming nitric acid (WFNA) for example, AB spontaneously ignites. A critical

parameter here is the time elapsed from the first contact between the oxidizer and the fuel to the appearance of flames. This is called the ignition delay (ID) and low values are essential to ensure proper operation in hypergolic engines.

Here, we present a proof-of-principle demonstration of experimental and theoretical performance characteristics of a new class of hypergols based on a metal–organic framework (MOF) design.[35–38] We have recently demonstrated how the combination of metal nodes such as Zn^{2+} and Co^{2+}, with linkers based on suitably substituted imidazoles (*e.g.* 2-vinyl and 2-acetylene-substituted imidazoles, **HVIm** and **HAIm**, respectively, Fig. 1a), results in zeolitic imidazolate frameworks (ZIFs)[39,40] exhibiting hypergolic behavior (Fig. 1b and c).

Specifically, these hypergolic MOFs (HMOFs) were found to exhibit ultrashort IDs (below 50 ms, and often below 5 ms) when in contact with traditional oxidizers such as white and red fuming nitric acids (WFNA, RFNA, respectively), along with heats of combustion (ΔH_C) around −8700 kJ mol^{-1}, with volumetric energy density (E_v) of 36.3 kJ cm^{-3}.[39] While these values are higher than for MMH (ΔH_C = −1304 kJ mol^{-1}; E_v = 24.7 kJ cm^{-3}) or UDMH (ΔH_C = −1979 kJ mol^{-1}; E_v = 25.9 kJ cm^{-3}),[39,41] HMOFs are also attractive as readily handled solids. They are stable in extended storage and do not exhibit ignition below at least 250–325 °C,[40] compared to AB who can self-ignites at temperature as low as 75 °C.[42]

As the next step in developing MOFs as a platform for new hypergolic systems, we demonstrate here that these HMOFs are highly effective additives to induce hypergolicity into conventional, non-hypergolic hybrid engine paraffin fuels. The hypergolic and energetic properties of HMOFs will be compared against additives currently used to bring these characteristics to hybrid fuels; AB and Al,[43] respectively.

2 Materials and methods

2.1 Hypergolic additives

The HMOFs used in this study were selected based on their hypergolic character. To ensure the safe operation of rocket engines using hypergolic propellants, an ID below 50 ms (ref. 44) is generally considered desirable, with ID below 10 ms required for dynamic altitude control systems.[33] However, with the hybrid propulsion approach, less stringent threshold can be used as the fuel is in a solid state and in a predetermined geometry. As a result, flooding of the engine is harder to achieve compared to a liquid engine, decreasing the likelihood of
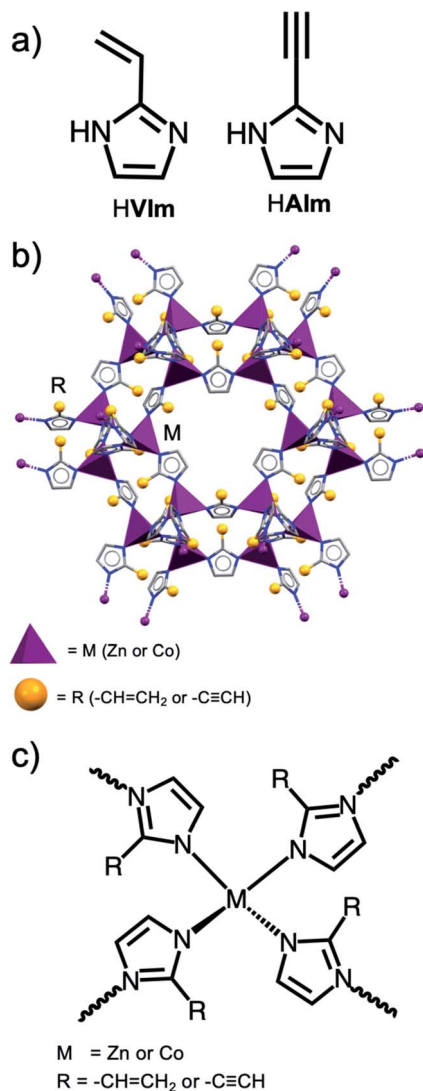
Fig. 1 (a) Schematic representation of the ligand used in this study. (b) A general illustration of the HMOFs. (c) A Schematic diagram of the assembly of metal ions and organic linkers to form HMOFs.

dramatic consequence in case of a high ID. It is not possible to add more fuel in the chamber than the exposed surface of the grain, making them safer than hypergolic liquid engines.

The IDs of hypergolic hybrid additives documented in the literature, including the HMOFs used here, are provided in Table 2. Previously reported RFNA and WFNA ignition drop tests on pure HMOFs samples revealed that the materials generated from H**AIm** exhibit the shortest ID values, at or below 5.0 ms. The HMOFs based on H**VIm** exhibit longer IDs, with Co(**VIm**)$_2$ at 11.0 (5.0) ms, and its zinc and cadmium analogues above 10 ms. These values compare advantageously with those of currently available hypergolic propellants or additives used for blending in hydrocarbon or polymeric matrices. More specifically, the H**AIm**-based HMOFs exhibit IDs matching that of hydrazines and AB. Even the worst-performing Cd(**VIm**)$_2$ exhibits an ID of 35.0 (1.0) ms at atmospheric pressure, notably shorter than the 50 ms target.[40] Other new HMOFs technologies, namely ZZU-362 and ZZU-363, were recently explored by Wang *et al.*[45] where hypergolic metal clusters were assembled with energetic ligands to create high density HMOFs, with IDs in the range of 26 to 60 ms.

2.2 Experimental section

2.2.1 Sample preparation. Hypergolic ignition tests on mixtures of HMOFs and paraffin were performed using Co(**VIm**)$_2$, Zn(**VIm**)$_2$ and Co(**AIm**)$_2$ as the hypergolic ignition additive, and FR5560 paraffin wax (The Candlewic Company, USA) as the matrix. The fuel samples were in the form of cylindrical pellets of approximately 300 mg, exposed to a single droplet of WFNA (10 μL volume) supplied using a glass syringe held approximately 150 mm above the pellets.

Ignition was investigated for three different sample configurations (configuration I, II and III), differing in how the HMOF and the FR5560 wax are combined. Configuration I was based on a fuel pellet made from homogeneous blend of 80 wt% FR5560 wax paraffin and 20 wt% HMOF. Configuration II consisted of a fuel pellet with a thin layer (*ca.* 10 mg by weight) of a HMOFs placed on top of it. In configuration III, a central hole was drilled in the pellets and filled with *ca.* 10 mg of a HMOF.

Samples for ignition testing in configuration I were made by melting the paraffin on a hot plate, followed by addition of a HMOF and gentle stirring until a homogeneous liquid is obtained. The blend was then poured into an aluminum mold and hand-pressed. Before ignition tests, the pellet surface was sanded using 80-grit sandpaper to ensure a consistent contact surface and exposure of hypergolic additives to the oxidizer

Table 2   Ignition delays of hypergolic additives and HMOFs with WFNA as the oxidizer

Category	Additive	Avg. ignition delay [ms]	Standard deviation [ms]	Ref.
Common hypergolic additive	AB	2.0	—	19
	Hydrazine	3.1	—	46
	Lithium–aluminum-hydride[a]	31.3	7.2	47
Metal–organic framework	ZZU-362	59.0	—	45
	ZZU-363	26.0	—	45
	Co(**VIm**)$_2$	11.0	5.0	40
	Zn(**VIm**)$_2$	29.0	1.0	—
	Co(**AIm**)$_2$	2.0	1.0	40
	Zn(**AIm**)$_2$	2.0	1.0	40

[a] Test conducted at a pressure of 0.10 MPa with analytical reagent-grade nitric acid (69.3 wt%).

droplet. Pellets were made one by one and, unless otherwise specified, ignition tests were performed in triplicate.

Samples for ignition testing in configuration II were prepared following the same steps as configuration I, followed by of pressing *ca.* 10 mg of a HMOF powder on the top surface of the pellet. Samples in configuration III were prepared by following the same steps as for configuration I. After solidification, a small hole of *ca.* 2 mm diameter and a depth of 4 mm was drilled in the center of the pellet, into which 10 mg of HMOFs powder was placed and gently pressed. Pellets for studies in configurations II and III were based either on pure paraffin, or on a mixture containing 20 wt% HMOFs with 80 wt% paraffin. In the latter case, both propellants were mixed together in the same way as for configuration I.

2.2.2 Droplet ignition tests. The ID was measured from the sequence of events following the impact of an oxidizer droplet on fuel samples, recorded using a Fastcam Mini AX200 high-speed camera (Photron, Japan) operating at 10 000 frames per second (fps). A 105 mm Sigma lens was used, set at an F-number of 1.4, with an exposure of 1/10 000 s and an OSL2 high-intensity light source (Thorlabs, USA). The ID was measured as the time interval between the initial contact of the droplet with the upper surface of a fuel pellet and the visible first emission of light. Previous experiments comparing visible light emission and OH* chemiluminescence in droplet ignition tests have revealed that the former can reliably be used to capture the onset of combustion.[34]

Table 3 Selected properties of HMOFs used here for comparison

Fuel Additive	Chemical Formula	Density [g cm^{-3}]	ΔH_f^0 [kJ mol^{-1}]
Co(**VIm**)$_2$	Co(C$_5$H$_5$N$_2$)$_2$	0.944	-1.3
Zn(**VIm**)$_2$	Zn(C$_5$H$_5$N$_2$)$_2$	0.976	-51.5
Co(**AIm**)$_2$	Co(C$_5$H$_3$N$_2$)$_2$	0.985	445.8
Zn(**AIm**)$_2$	Zn(C$_5$H$_3$N$_2$)$_2$	0.996	397.1

2.2.3 Ignition of mixtures of HMOFs and paraffin. A sequence of images representative of the ignition of samples of pure HMOFs is illustrated in Fig. 2. In each sequences, the second image captures the first contact between the oxidizer droplet and the sample, while the image directly after represents the first recorded frame where ignition is visible. Any subsequent images are shown as a means to illustrate the intensity and character of the flame. In the case of Zn(**VIm**)$_2$ (Fig. 2b), only small sparks were perceptible, in contrast to the sustained flames observed with the two other HMOFs.

For the ignition tests conducted on samples containing the paraffin and a HMOF, the results are summarized in Table 4.

2.2.4 Periodic DFT calculations. Periodic density functional theory (DFT) calculations were used to determine the standard enthalpies of formation (ΔH_f^0) of ZIF materials. In order to calculate the ΔH_f^0 values, electronic energies of elements in their standard states (Zn and Co metals, graphite, H$_2$, N$_2$ and O$_2$ gases) had to be combined with the electronic
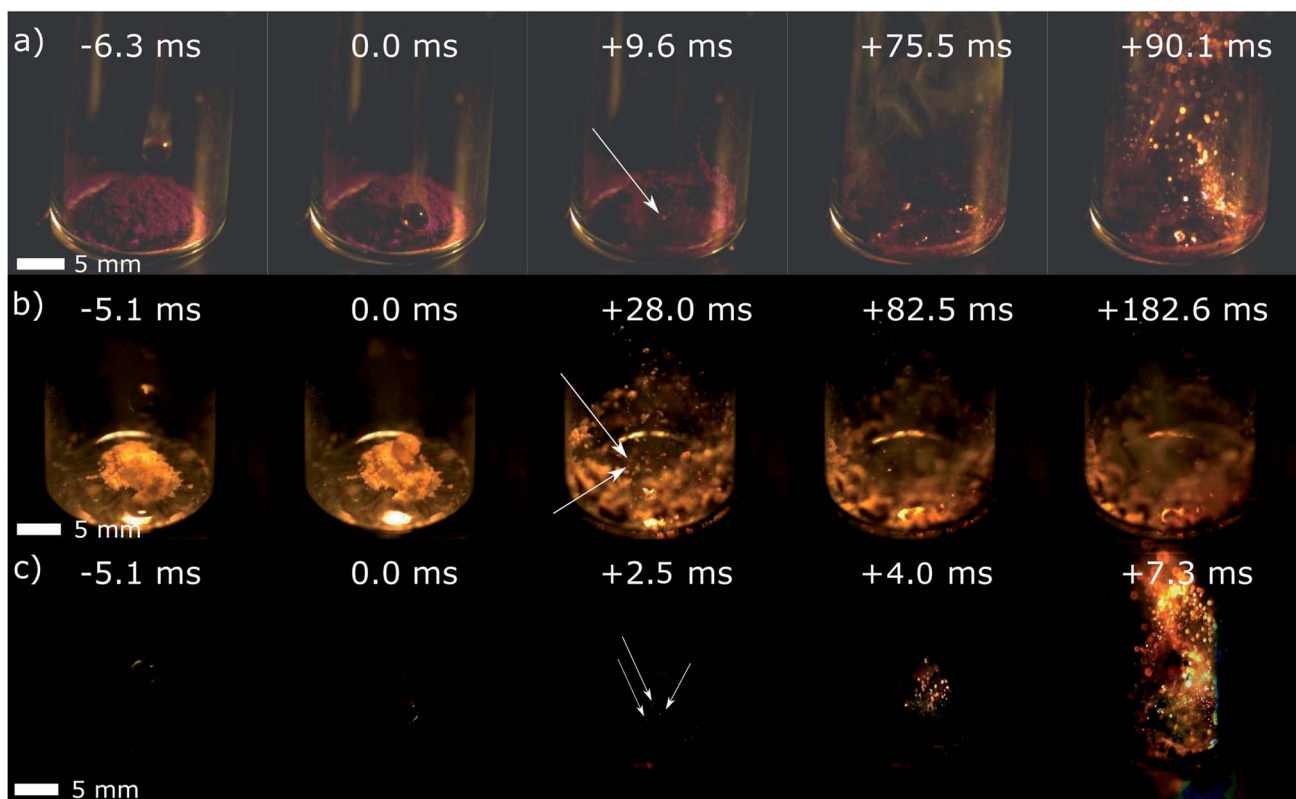

Fig. 2 Droplet ignition tests on (a) pure Co(**VIm**)$_2$, (b) pure Zn (**VIm**)$_2$, and (c) pure Co(**AIm**)$_2$ using *ca.* 10 mg of HMOF powder samples and WFNA as the oxidizer. The location of the first ignition is marked with the white arrow. Picture in (c) were digitally modified to remove reflections on the glass vial. The original videos are available online as ESI.†
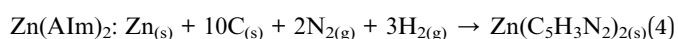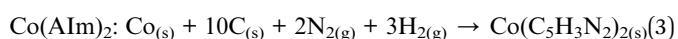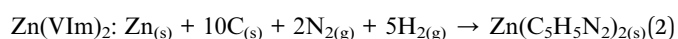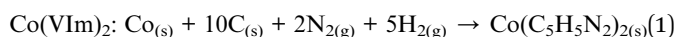
Table 4 Ignition delay of tested fuel formulations and configuration using WFNA as the oxidizer. Configuration I = Fuel pellet, Configuration II = HMOF powder layer on fuel pellet, Configuration III = HMOF powder-filled hole in fuel pellet. NT = Not Tested. — = No ignition

MOF	Configuration	Pellet content	Avg. ignition dlay [ms]	Standard deviation [ms]
Co(**VIm**)$_2$	I	80 wt% FR5560 wax/20 wt% Co(**VIm**)$_2$	—	—
		50 wt% FR5560 wax/50 wt% Co(**VIm**)$_2$	—	—
	II	100 wt% FR5560 wax	12.9	10.7
		80 wt% FR5560 wax/20 wt% Co(**VIm**)$_2$	13.3	5.3
	III	100 wt% FR5560 wax	6.3	1.6
		80 wt% FR5560 wax/20 wt% Co(**VIm**)$_2$	8.3	0.1
Zn(**VIm**)$_2$	I	80 wt% FR5560 wax/20 wt% Zn(**VIm**)$_2$	NT	NT
		50 wt% FR5560 wax/50 wt% Zn(**VIm**)$_2$	—	—
	II	100 wt% FR5560 wax	—	—
		80 wt% FR5560 wax/20 wt% Zn(**VIm**)$_2$	—	—
	III	100 wt% FR5560 wax	—	—
		80 wt% FR5560 wax/20 wt% Zn(**VIm**)$_2$	—	—
Co(**AIm**)$_2$	I	80 wt% FR5560 wax/20 wt% Co(**AIm**)$_2$	—	—
		50 wt% FR5560 wax/50 wt% Co(**AIm**)$_2$	7.0[a]	1.8[a]
	II	100 wt% FR5560 wax	2.3	0.1
		80 wt% FR5560 wax/20 wt% Co(**AIm**)$_2$	NT	NT
	III	100 wt% FR5560 wax	1.8	0.7
		80 wt% FR5560 wax/20 wt% Co(**AIm**)$_2$	NT	NT

[a] Tested in the form of powder since the mixture was too brittle to form a pellet.

energies of ZIF structures from our previous publication.[40] Calculations were performed with the plane wave DFT code CASTEP 16.1.[48] The crystal structures of ZIFs, Zn, Co and Cd metals were converted into CASTEP input format using the program CIF2Cell.[49] For the elements present in the gas phase under standard conditions (H_2, N_2) the respective molecules were placed in a $30 \times 30 \times 30$ Å cubic box, sufficiently large to prevent the interaction for the periodic images of gas molecules. Calculations were performed using a PBE[50] functional combined with Grimme D2 dispersion correction.[51] The plane-wave basis set was truncated at 750 eV cutoff, and norm-conserving pseudopotentials were used to attenuate the core regions of electron density. In the case of crystal structures, optimization involved relaxation of atom coordinates and unit cell parameters, subject to the symmetry constraints of the corresponding space groups. In the case of gas phase molecules, the dimensions of the cubic box were kept fixed throughout the optimization. The optimization was deemed converged upon satisfying the following criteria: a maximum energy change of 10–5 eV per atom, a maximum force on atom of 0.01 eV Å^{-1}, a maximum atom displacement of 0.001 Å, and a residual stress of 0.05 GPa (only for variable cell optimization for crystal structures).

The resulting energies were used to compute the enthalpies of formation according to the following reaction equations:

$$Co(VIm)_2: Co_{(s)} + 10C_{(s)} + 2N_{2(g)} + 5H_{2(g)} \rightarrow Co(C_5H_5N_2)_{2(s)} \quad (1)$$

$$Zn(VIm)_2: Zn_{(s)} + 10C_{(s)} + 2N_{2(g)} + 5H_{2(g)} \rightarrow Zn(C_5H_5N_2)_{2(s)} \quad (2)$$

$$Co(AIm)_2: Co_{(s)} + 10C_{(s)} + 2N_{2(g)} + 3H_{2(g)} \rightarrow Co(C_5H_3N_2)_{2(s)} \quad (3)$$

$$Zn(AIm)_2: Zn_{(s)} + 10C_{(s)} + 2N_{2(g)} + 3H_{2(g)} \rightarrow Zn(C_5H_3N_2)_{2(s)} \quad (4)$$

2.3 Ignition results and discussion

2.3.1 Ignition tests of blends with Co(VIm)$_2$. Drop tests on pellets containing 20 wt% Co(**VIm**)$_2$ with 80 wt% paraffin in configuration I generated only discrete, small sparks on the pellet surface, with no definitive ignition. Moreover, the sparks were difficult to distinguish from light reflection on the surface of the WFNA droplet, preventing the clear measurement of IDs. This difficulty to observe flames in configuration I is most likely caused by the very fine granulometry of the HMOF powders used to prepare the samples, with an average particle size on the order of 0.1 μm.[40] When embedded in a paraffin matrix, the weak outgassing produced by these very small particles is quenched by the oxidizer layer resting on top of the fuel pellet.

To achieve ignition, we explored using a single pellet containing 50 wt% Co(**VIm**)$_2$ and 50 wt% paraffin wax. In this case, a strong reaction occurred on the surface of the pellets, with bubbles and gas generation 100.8 ms after the first contact with the WFNA droplet. The herein used pellet fabrication method, in which the HMOFs are mixed with melted paraffin, could hinder hypergolic ignition at low loadings, due to the paraffin completely coating the very fine particles and shielding them from the oxidant. Ignition of paraffin requires vaporization through the exothermic hypergolic ignition upon contact of the HMOF with WFNA. In configuration I, the heat produced from the weak outgassing is lost to the WFNA liquid layer resting on top of the pellet. Several seconds after the test, each pellet was thoroughly examined: a black layer of burned HMOFs was present on its surface, hinting that some HMOFs reacted with the oxidant, but that this reaction was indeed quenched before triggering the combustion of paraffin.

Drop tests in configuration II revealed ignition in all cases, accompanied with large bursts of flame visible in half of all the tests performed. Bursts of flame occurred mainly on top of the

pellets and are attributed to the hypergolic ignition of the HMOF upon contact with WFNA. Overall, the experiments suggest that the HMOF flame did not transition to a paraffin flame and that the paraffin did not react with WFNA. The hypergolic ignition in this case also does not appear to generate enough heat to melt the paraffin and create a sustained flame, most likely because of the small particle size in the HMOF layer. Due to the impact of the WFNA droplet, part of the HMOF layer was expelled away from of the paraffin pellet, which decreased the opportunity for ignition of the paraffin. In this configuration, and using Co(**VIm**)$_2$ as the HMOF, a large variation in IDs was observed, which we believe might be related to other factors not evaluated here, such as the compactness or the uniformity of the HMOF layer. These two parameters will affect the spreading of the HMOF layer upon impact with the oxidizer droplet.

To test the hypothesis of HMOF particles being too small, we explored hypergolic ignition in configuration III. In 5 out of 6 cases, using either neat paraffin or a blend of paraffin and Co(**VIm**)$_2$ in respective weight ratio 80 : 20, sparks were produced, followed by bursts of flames resembling those observed for configuration II. However, the bursts of flame in configuration III were also followed by continuous combustion (up to 2.5 s) that was attributed to the paraffin, first reacting with the leftover WFNA and then with ambient air. This interesting result indicated that the addition of HMOFs in the fuel matrix did not significantly hinder the ignition of the paraffin, thus confirming that combustion is not affected after the hypergolic reaction. Using 5 mg Co(**VIm**)$_2$ instead of 10 mg in this configuration did not lead to the ignition of the paraffin.

Notably, the ignition with Co(**VIm**)$_2$ in configuration III, using either pure paraffin and or HMOF-paraffin blends as the pellet material, produced remarkably short average IDs of respectively 6.3 (1.6) ms and 8.3 (0.1) ms. These values are 52% and 37% shorter, respectively, than the IDs seen in configuration II, confirming that spatially concentrated HMOF not only enable paraffin ignition, but also reduce the ID value. One of the major differences between both configurations is the reduction of the amount of HMOF particles expelled from the pellet upon contact with the droplet in configuration III. Concentrated in the center of the pellet, the HMOF flame contributed more to the vaporization of the paraffin through longer flame and direct contact with the edges of the hole. Furthermore, eight out of twelve tests in configurations II and III were observed to ignite

with IDs below 10 ms, which is considered to be the target value for dynamic altitude control systems.[33]

2.3.2 Ignition tests on blends with Zn(VIm)$_2$. Tests carried with Zn(**VIm**)$_2$ did not lead to the ignition of the pellets in any of the three configurations. In some cases, mostly under configurations II and III, a reaction occurred on the surface of the pellet: fumes were generated and a layer of black material was observed to form. Furthermore, small sparks similar to those observed on pure Zn(**VIm**)$_2$ powder (Fig. 2c) were observed. However, due to the difficulty of distinguishing the light emitted by the sparks from the light refracted by the WFNA droplet, ID values are not reported.

A single droplet test was performed with a pellet containing 50 wt% paraffin wax and 50 wt% Zn(**VIm**)$_2$ under configuration I. Since sparks were not observed in that case, ignition of mixtures containing 20 wt% of Zn(**VIm**)$_2$ was not tested.

The poor hypergolic performance of Zn(**VIm**)$_2$-paraffin blends compared to those based on Co(**VIm**)$_2$ did not warrant further experiments. This result was consistent with our previous observation[40] of lower hypergolic reactivity for HMOFs based on zinc, compared to cobalt.

2.3.3 Ignition tests on blends with Co(AIm)$_2$. As Co(**AIm**)$_2$ has previously been demonstrated to be the most rapidly igniting HMOF so far, tests were conducted only in configurations II and III, using a neat paraffin wax pellet. Tests in configuration I could not be done using a pellet, as the mixture of HMOF and paraffin was too brittle after being pressed by hand. Consequently, the drop ignition tests in this configuration were conducted on a mixture of Co(**AIm**)$_2$ and paraffin powder. Out of the three tests carried that way, two led to hypergolic ignition lasting approximately 2 seconds, making Co(**AIm**)$_2$ the only HMOF that readily ignited even in a homogeneous powder mixture with paraffin (Fig. 3).

Tests carried with Co(**AIm**)$_2$ in configuration II all revealed rapid ignition, with an average ID of 2.3 (0.1) ms, which corresponds to a reduction of 82% compared to Co(**VIm**)$_2$ in the same configuration. In addition to a remarkably short ID values, well under the 10 ms target value, paraffin ignition and burning was observed in two out of three tests (Fig. 4). Compared to Co(**VIm**)$_2$, the herein observed ignition of paraffin bearing a thin layer of Co(**AIm**)$_2$ may be attributed to a faster hypergolic reaction with WFNA, leading to more heat being transferred to the paraffin before the HMOF particles were expelled from the surface. Overall, these results clearly demonstrate that the heat
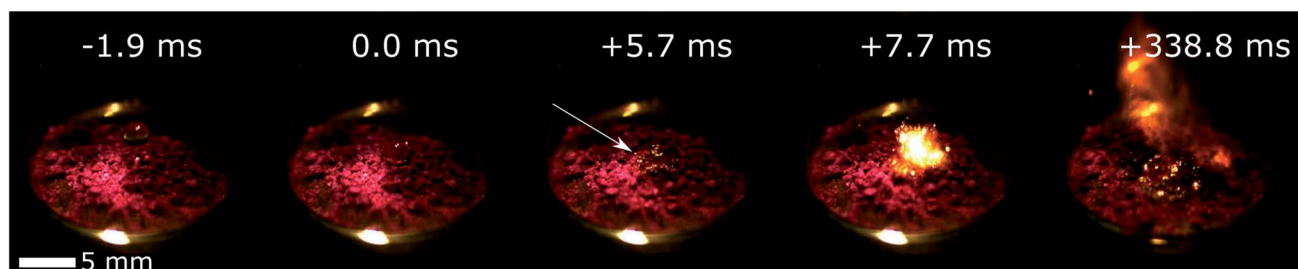

Fig. 3 Example of a ignition drop test on 50 wt% FR5560 wax/50 wt% Co(**AIm**)$_2$ using WFNA as the oxidizer. The location of the first ignition is marked with the white arrow. Full sequence available on ESI.†
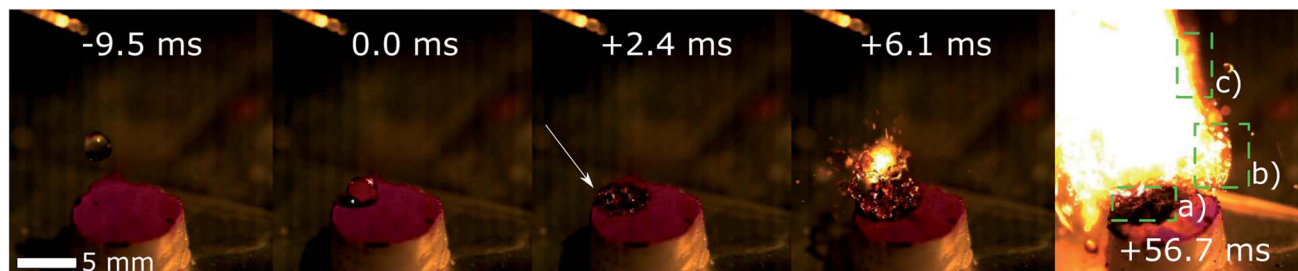
Fig. 4 Example of an ignition drop test on a FR5560 wax pellet covered with a thin 10 mg layer of Co(**AIm**)$_2$ (configuration II), using WFNA as the oxidizer. The location of the first ignition is marked with the white arrow. (a) Burned paraffin and HMOFs. (b) Burning HMOF. (c) Paraffin flame. Full sequence available in ESI.†

released by hypergolic ignition of a thin layer of Co(**AIm**)$_2$ can be used to ignite solid paraffin fuel underneath.

Ignition drop tests with Co(**AIm**)$_2$ in Configuration III gave the shortest ID values, leading to an average of 1.8(0.7) ms. This value represents a decrease of 71% compared to the results obtained with Co(**VIm**)$_2$ in the same configuration. Notably, following the initial hypergolic ignition of Co(**AIm**)$_2$, paraffin ignition was observed in all cases (Fig. 5).

3 Theoretical performance

The use of MOFs as modular propellant fuels and additives is contingent upon their projected performance as components of fuel blends useful for practical engine designs. In that context, we present here the theoretical performance of HMOFs as additives for hypergolic ignition in hybrid propulsion systems based on paraffin fuel. The thermo-chemical simulations considered solid paraffin wax for the fuel grain matrix, and the performance characteristics were calculated for variable HMOF additive mass fractions and O/F ratios. A paraffin-based propellant system was selected for modeling as its liquefying characteristics results in the high regression rates needed for high-thrust hybrid rocket engines.

The I_{sp} and density specific impulse (ρI_{sp}) are propulsive performance parameters heavily dependent on a variety of physical factors such as engine and nozzle geometries as well as on the fuels and oxidizers used. The exhaust gas velocity V_e is a critical parameter in the calculation of the I_{sp}. So it is a function of the temperature of combustion T_c, the mean molecular

weight of the exhaust gas M_W, the ratio of the exit pressure and combustion pressure $\frac{P_e}{P_c}$ and the ratio of specific heat γ:

$$I_{sp} = \frac{V_e}{g} = \frac{1}{g}\sqrt{\frac{2\gamma R_u T_c}{(\gamma-1)M_W}\left(1 - \frac{P_e}{P_c}\right)^{\frac{\gamma-1}{\gamma}}} \quad (5)$$

Thus, the higher the combustion pressure and temperature, and the lower the molecular weight of the combustion gas, the higher the performance of the engine will be.

The density specific impulse measures the performance of a given propellant by taking into account its density, with higher density specific impulse associated with higher engine performance for a given volume of propellant. It is defined by:

$$\rho I_{sp} = \rho_{prpopellant} \cdot I_{sp} \quad (6)$$

with $\rho_{propellant}$ defined as:

$$\rho_{propellant} = \frac{\rho_{ox} \cdot \rho_{fuel}(1 + O/F)}{\rho_{fuel} \cdot O/F + \rho_{ox}} \quad (7)$$

where ρ_{ox} is the density of the oxidizer and ρ_{ox} is the density of the fuel. The density specific impulse is determined at the optimal O/F for each fuel and oxidizer formulation.

Finally, the C^* values are a mean to assess the combustion independently of the nozzle efficiency or performance. The value of C^* is proportional to the I_{sp} and is defined by:

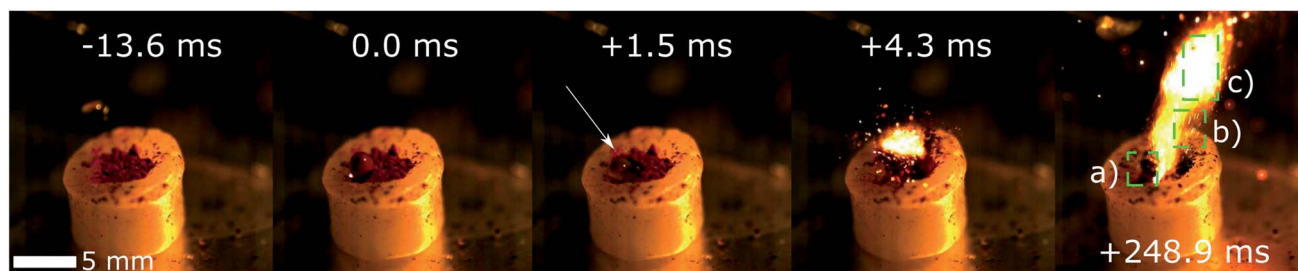$$C^* = P_c \cdot A_t \frac{\cdot}{m} \quad (8)$$

Fig. 5 Drop tests on neat paraffin wax pellet with a 10 mg of Co(**AIm**)$_2$ located in a hole in the center, using WFNA as the oxidizer. The location of the first ignition is marked with the white arrow. (a) Burned paraffin and HMOF. (b) Burning HMOF powder. (c) Paraffin flame. Full sequence available in ESI.†

where A_t is the throat area of the nozzle and $\dot{m}$ is the average mass flow of the engine.

The I_{sp} and ρI_{sp} of hybrid paraffin-based fuel mixtures containing HMOFs were calculated using the NASA-CEA software.[52] The values obtained were then compared to those for paraffin fuels containing AB and aluminum for reference. AB in a paraffin matrix can yield hypergolic ignition,[14,19,34] just as our proposed use of HMOFs. Although aluminum particles as fuel additives do not yield hypergolicity, they were considered here for comparison as energetic rocket fuel additives.[43] The oxidizers investigated were WFNA, LO_x and high-test peroxide (HTP, H_2O_2 at 90 wt% concentration in H_2O). The absolute combustion chamber pressure considered was 6.89 MPa (1000 psia) and the exhaust gases were assumed to be in chemical equilibrium conditions and perfectly expanded to atmospheric pressure. The properties of the oxidizers were retrieved from NASA-CEA, with the densities used for calculations being 1.141 g cm^{-3} for LO_x, 1.513 g cm^{-3} for WFNA and 1.392 g cm^{-3} for HTP. The chemical formula of the paraffin used for the analysis is $C_{32}H_{66}$ with an approximate density of 0.90 g cm^{-3}. The properties of paraffin, aluminum and AB were extracted from the NASA-CEA library whereas those of the HMOFs were measured experimentally and reported earlier in Table 3.

3.1 Performance of pure HMOFs

For comparison purposes, theoretical performances of pure fuel matrices made of paraffin and HTPB without energetic or hypergolic additives are shown in Fig. 6 and Table 5, as a function of the O/F ratio for various oxidizers. When used as the oxidizer, LO_x used as oxidizer provides the best specific impulse among those presented with a maximal value of approximately 300 s. The use of WFNA allowed maximal values of I_{sp} of approximately 265 s whereas engines using H_2O_2 could achieve an I_{sp} of almost 290 s.

Before assessing the performances of HMOFs within a paraffin fuel matrix, the I_{sp} was calculated for their pure form and was compared to the values for aluminum and AB. These results are presented for Co($\textbf{AIm}$)$_2$ and Co($\textbf{VIm}$)$_2$ in Table 6. With all oxidizers studied, pure AB always presented the highest

Fig. 6 Theoretical performances of common propellants and oxidizers used in hybrid rocket engines. Equilibrium conditions, chamber pressure of 6.89 MPa and perfect expansion to atmospheric conditions.

Table 5 Theoretical performances of commonly used fuels and oxidizer combinations at their optimum O/F ratio

Fuel	Oxidizer	O/F	I_{sp} [s]	ρI_{sp} [sg cm^{-3}]
HTPB	WFNA	4.5	265.1	360.0
HTPB	LO_x	2.3	301.2	321.5
HTPB	H_2O_2 90 wt%	6.7	289.2	378.1
Paraffin	WFNA	5.0	264.4	359.3
Paraffin	LO_x	2.6	301.8	321.0
Paraffin	H_2O_2 90 wt%	7.4	289.0	377.7

specific impulse. Pure Co($\textbf{AIm}$)$_2$ and Co($\textbf{VIm}$)$_2$ had slightly lower I_{sp} values compared to AB but were always higher than pure aluminum. As expected, aluminum yielded a higher ρI_{sp} compared to AB and the selected HMOFs because of its high density. Interestingly, the ρI_{sp} of Co($\textbf{AIm}$)$_2$ and Co($\textbf{VIm}$)$_2$ was higher than AB when WFNA or HTP were used as the oxidizer.

3.2 Performance of HMOFs/Paraffin fuels

In Table 7, the results for HMOF-containing fuels are shown side-by-side with the values calculated for fuel blends containing AB or aluminum. Fig. 7a and b present the I_{sp} and ρI_{sp} of paraffin-based fuels as a function of additive mass loading, with WFNA as the oxidizer. For each additive mass fraction, calculations were done over a broad range of O/F ratios and the one yielding the highest I_{sp} was chosen as optimal and reported in the figures and in Table 7. A solid additive mass loading range of 5 wt% to 50 wt% was considered; the upper-bound was selected because homogeneous blends were experimentally achieved up to 50 wt% for a wide variety of additives[32] with higher concentration yielding very brittle fuel blends. However, in practical applications with paraffin fuel matrices, desirable burning characteristics may only be present over a reduced mass loading range. At high mass loads, the inclusion of additives could lead to decreased performances and fuel
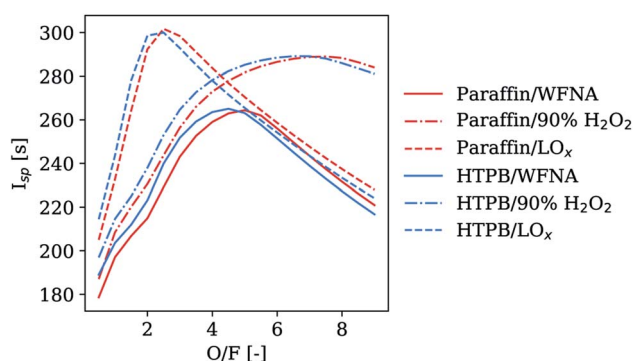
Table 6 Theoretical performances of pure MOFs, aluminum and ammonia borane. Equilibrium conditions, chamber pressure of 6.89 MPa and perfect expansion to atmospheric conditions are assumed

Oxidizer	Fuel	O/F	I_{sp} [s]	ρI_{sp} [sg cm^{-3}]
WFNA	AB	1.00	288.67	297.14
	Aluminum	2.00	231.88	411.05
	Co($\textbf{VIm}$)$_2$	2.50	242.01	312.35
	Zn($\textbf{VIm}$)$_2$	2.50	241.83	316.17
	Co($\textbf{AIm}$)$_2$	2.25	245.24	318.50
LO_x	AB	1.75	316.62	309.22
	Aluminum	2.25	228.32	316.79
	Co($\textbf{VIm}$)$_2$	1.25	261.16	272.69
	Zn($\textbf{VIm}$)$_2$	1.25	264.04	280.21
	Co($\textbf{AIm}$)$_2$	1.25	263.48	280.86
H_2O_2 90 wt%	AB	1.25	298.04	307.61
	Aluminum	2.75	269.86	431.37
	Co($\textbf{VIm}$)$_2$	3.75	271.13	343.13
	Zn($\textbf{VIm}$)$_2$	3.75	270.95	346.10
	Co($\textbf{AIm}$)$_2$	3.50	272.80	347.81

Table 7 Combustion characteristics of AB, Al and HMOFs additives in a paraffin matrix at a mass loading of 20 wt%. Equilibrium conditions, chamber pressure of 6.89 MPa and perfect expansion to atmospheric conditions are assumed

Oxidizer	Additive	O/F	C^* [m s^{-1}]	T_C [K]	M_W [g mol^{-1}]
WFNA	AB	4.1	1616.1	3105.95	24.729
	Aluminum	3.4	1614.5	2905.89	23.916
	Co(**VIm**)$_2$	4.5	1571.8	3131.48	27.299
	Zn(**VIm**)$_2$	4.5	1573.9	3139.94	27.351
	Co(**AIm**)$_2$	4.0	1585.8	3123.26	26.029
LO$_x$	AB	2.1	1836.1	3503.93	21.942
	Aluminum	1.7	1814.9	3623.51	22.662
	Co(**VIm**)$_2$	2.4	1771.5	3660.30	26.021
	Zn(**VIm**)$_2$	2.3	1781.9	3652.10	25.388
	Co(**AIm**)$_2$	2.1	1789.9	3594.36	24.232
H$_2$O$_2$ 90 wt%	AB	5.8	1754.4	3065.08	20.805
	Aluminum	5.0	1749.0	3164.18	21.496
	Co(**VIm**)$_2$	5.7	1730.1	3062.22	21.441
	Zn(**VIm**)$_2$	5.7	1732.4	3070.17	21.467
	Co(**AIm**)$_2$	5.7	1732.2	3075.78	21.538

regression rates. For instance, using AB as an hypergolic additive, Weismiller *et al.* reported that at concentration over 20% by mass in a paraffin or a HTPB fuel matrix, the regression rate was reduced due to a condensed phase created on the surface of the fuel grain during the combustion process.[14] Condensed phase products on the surface of the pellets were also observed with all HMOFs investigated in this paper. This reduction in regression rate is therefore also expected with HMOFs. For this reason, a moderate mass loading of 20 wt% was selected to investigate the effect of the O/F ratio on the I_{sp}, with results presented in Table 7 and in Fig. 7c when WFNA is used as the oxidizer.

As shown in Fig. 7a and b, both I_{sp} and ρI_{sp} are slightly lower when HMOFs were added to the fuel mixture compared to pure paraffin reacting with WFNA, decreasing approximately linearly with increasing MOF loading. This contrasts with the use of AB, which resulted in a slight increase in I_{sp}. The addition of aluminum also yielded an increase in I_{sp}, an effect scaling

approximately linearly with increased additive mass loading (an increase of 3.3% at a mass load of 50 wt%). Although there was a minor reduction in I_{sp} on the order of 2.0% at a mass load of 50 wt% for the HMOF-containing fuels compared to pure paraffin as well as paraffin-AB or -Al mixtures, this modest performance tradeoff implied that HMOFs could be useful as additives to impart hypergolicity to an otherwise non-hypergolic fuel.

The performance parameters were also calculated using LO$_x$ as an oxidizer, with the results shown in Fig. 8a, yielding higher values compared to WFNA. Additionally, the decrease in I_{sp} and ρI_{sp} values associated with increasing the HMOF mass loading was less pronounced when LO$_x$ was used in calculations. For instance, when using LO$_x$ the decrease of I_{sp} for Zn(**AIm**)$_2$ at a fixed mass load of 20 wt%, was 2.15% and 1.18% compared to AB and Al, respectively. Corresponding values were 1.53% and 1.84%, respectively, when WFNA was used. Interestingly, behavior of the calculated I_{sp} as a function of the O/F ratio for the HMOFs revealed a very similar combustion behavior to the fuel blends using AB and Al as additives, again considering a case with 20% mass loading (Fig. 8c). The curves were all similar in profile, with maxima close to an O/F ratio of 2.5 in all cases. Notably, the I_{sp} values for Zn(**AIm**)$_2$ and AB are almost equal and just under 300 s at an O/F ratio of approximately 2.5.

Finally, the same parameters were calculated using HTP as an oxidizer (Fig. 9). Overall, the I_{sp} of the hypergols was similar to those obtained when using LO$_x$ as an oxidizer. However, there was a smaller drop in I_{sp} with increasing HMOF mass loading. At a mass loading of 20 wt%, the decrease was of 0.98% and of 1.07% when compared to AB and Al, respectively, at the same mass loading. However, the ρI_{sp} with 90% HTP was higher than that when using WFNA as the oxidizer. The trends for the variation of the I_{sp} as a function of the O/F again showed very similar combustion behavior between the HMOFs, AB and Al additives.

In addition to the I_{sp} and ρI_{sp} calculated using the NASA-CEA software, the C^* values were also computed. The values are
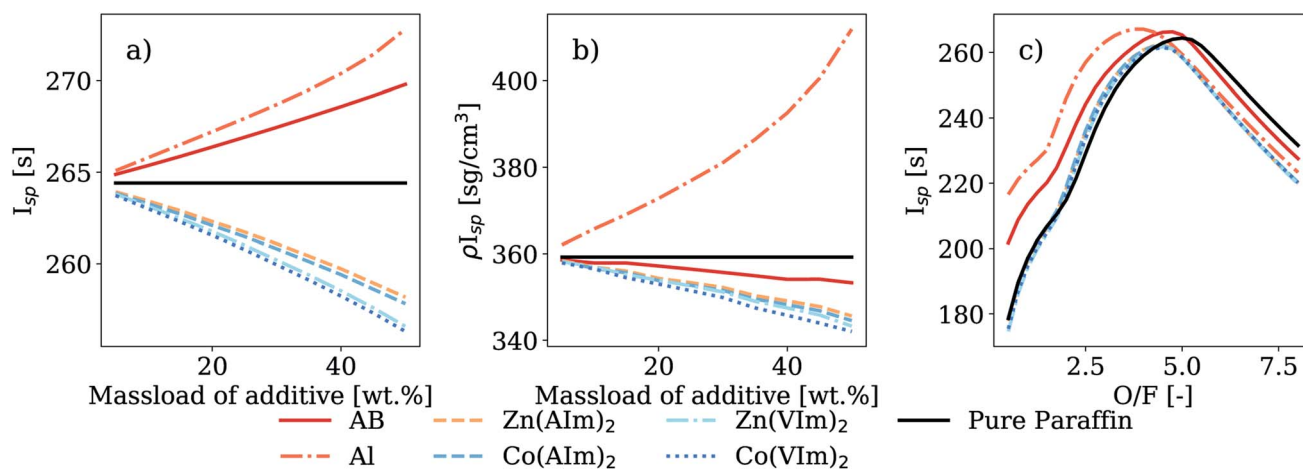

Fig. 7 (a) Specific impulse as a function of the mass load of additive in a paraffin-based fuel matrix at the optimal O/F ratio, (b) density specific impulse as a function of the mass load of additive in a paraffin-based fuel matrix and (c) theoretical performance at 20 wt%, as a function of oxidizer-to-fuel ratio. Calculated using WFNA as the oxidizer.
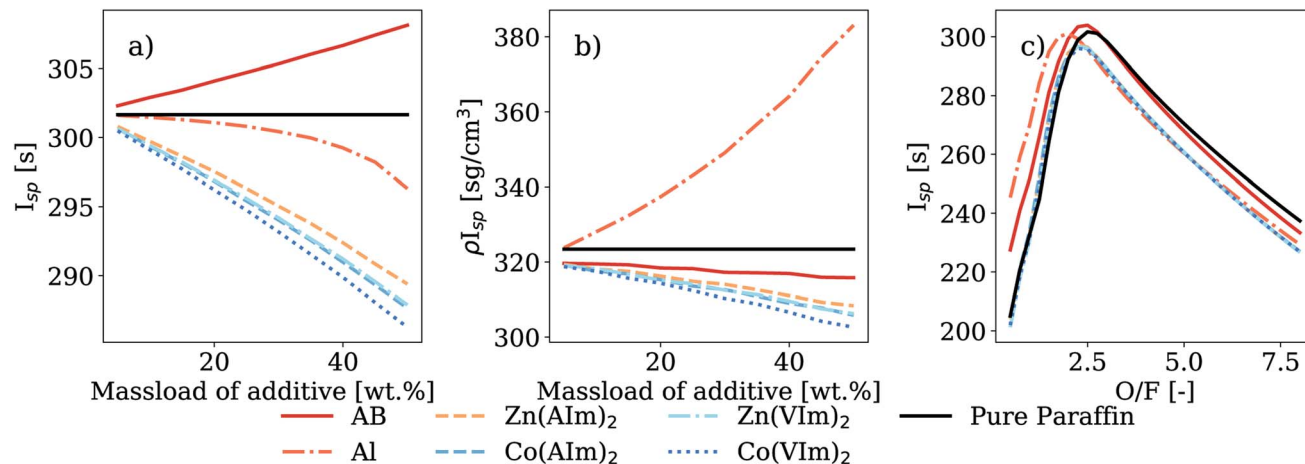
Fig. 8 (a) Specific impulse as a function of the mass load of additive in a paraffin-based fuel matrix at the optimal O/F ratio, (b) density specific impulse as a function of the mass load of additive in a paraffin-based fuel matrix and (c) theoretical performance at 20 wt%, as a function of oxidizer-to-fuel ratio. Calculated using LO_x as the oxidizer.

reported in Table 7 for a mass loading of 20 wt% in a paraffin matrix, in each case for the O/F ratio that provides the maximum C^* value. The combustion temperature corresponds to the temperature inside the combustion chamber, whereas the molecular weight was computed at the exit of the nozzle and took into account products in condensed phases.

The results presented here showed that for the HMOF considered, the C^* and optimal O/F were similar. The latter was also comparable to the optimal O/F when AB was used as the additive. Interestingly, when LO_x was used as the oxidizer, every paraffin-additive mixtures had a higher C^* than the previously mentioned RP1-LO_x (1774 m s^{-1}) and N_2O_4-UMDH/hydrazine (1711 m s^{-1}) fuel–oxidizer combinations. When considering 90% HTP as the oxidizer, the C^* values for the HMOFS were also higher than for the N_2O_4-UMDH/hydrazine combinations. In general, combustion of paraffin and HMOFs yielded a higher combustion temperature compared to AB, while surpassing

aluminum when WFNA was used as the oxidizer. Even though the temperature of combustion of HMOFs was higher than AB, the specific impulse of the latter was higher, primarily due to the lower molecular weight of the exhaust gases.

4   Discussion

The presented results demonstrate significant potential of HMOFs as solid, safe to handle and hydrazine- or aminoborane-free additives that can provide hypergolicity to inexpensive, safe and energy-dense solid hydrocarbon fuels required for use in hybrid rocket engines, such as paraffin. The I_{sp} values calculated are closed to those obtained when aluminum metal or AB is included in the paraffin matrix. For instance, with a moderate mass loading of 20 wt% for which good combustion efficiency and regression rates are expected, the relative penalty in I_{sp} is not more than 2.15%, compared to the use of hypergolic AB or
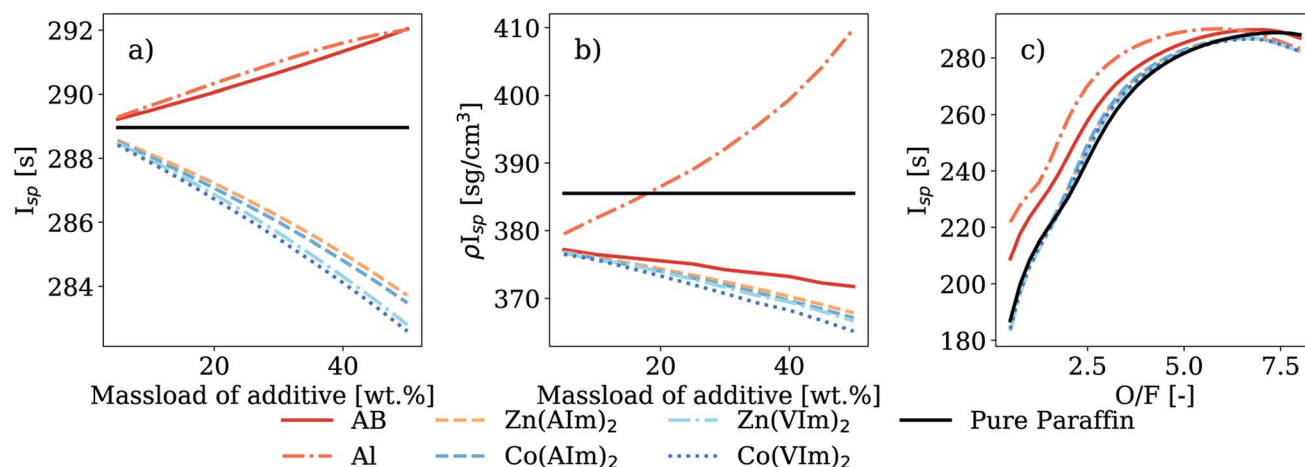

Fig. 9 (a) Specific impulse as a function of the mass load of additive in a paraffin-based fuel matrix at the optimal O/F ratio, (b) density specific impulse as a function of the mass load of additive in a paraffin-based fuel matrix and (c) theoretical performance at 20 wt%, as a function of oxidizer-to-fuel ratio. Calculated using 90 wt% H_2O_2 as the oxidizer.

non-hypergolic Al additives, when LO_x is used as the oxidizer. This slightly higher specific impulse for the hypergolic AB – WNFA combination compared to the HMOFs investigated here is explained by the very high hydrogen content of the former resulting in a lower molecular weight of the combustion products, even though HMOFs have a large heat of combustion. Another minor disadvantage for the use of HMOFs as fuel additives compared to AB or Al is the slightly narrower range of O/F ratios over which the I_{sp} is close to its optimal value. This means that with HMOF additives in hybrid engines, the oxidizer supply would need to be more carefully controlled and evenly distributed over the fuel grain to ensure optimal combustion, especially when using WFNA. As shown in Fig. 7c, the I_{sp} as a function of the O/F ratio for HMOF-based paraffin mixtures features a slightly sharper peak between 3.50 and 4.25, as opposed to the broader peaks observed both AB and aluminum additives. However, this difference between the behavior of the additives is much less pronounced when LO_x or 90% HTP are used as oxidizers.

A hybrid engine relying on HMOFs to provide hypergolicity to paraffin or other hydrocarbon fuel matrices would therefore lose slightly in I_{sp}, but gains in having a simple ignition, eliminating the need for more complex external ignition systems. Hypergolic propellants can also add flexibility with regards to possible mission profiles, as they could enable reliable restartability, a feature not possible for solid rockets and adding complexity to non-hypergolic hybrids. A caveat is the difficult ignition observed when the very fine HMOF powders were evenly mixed with paraffin. In droplet ignitions test shown here, the mixture composition surrounding MOF particles immersed in the fuel matrix is very lean and as a result the hot outgassing that might initiate the combustion can be quenched by the local over-abundance of oxidizer. In engine conditions, careful tuning of the O/F ratio during the transient ignition phase of operation could avoid this problem, but this observation highlights the necessity to carefully assess the importance of granulometry of the additives on the hypergolic ignition phenomena in hybrid engines.

Compared to the reference hypergolic additive for hybrid rocket propulsion, AB, HMOFs have the potential to be much easier to mix with paraffin and other hydrocarbons. This is explained by the presence of organic ligands and by their much higher temperature of decomposition, determined by thermogravimetric analysis to be 250–325 °C (ref. 40) for the HMOFs considered here, and 80–100 °C for AB.[42] HMOFs also have lower toxicity compared to hypergolic fuels based on hydrazine, meaning they offer a safer and less toxic alternative additive that is easier to handle. Finally, HMOFs have the ability to be tailored as needed by including other metals or chemical compounds in their porous structure, making them suitable for a wide range of needs.

5 Conclusions

We have outlined the development of a new materials platform for hypergolic hybrid rocket propulsion, based on metal–organic frameworks (MOFs) as a recently emerged class of hypergolic materials. The hypergolic MOFs exhibit ignition delays and energy content competitive with currently used fuels and additives, and this case study has shown that the presence of Co(**AIm**)$_2$ and Co(**VIm**)$_2$ can enable reliable and short ignition delays (below 10 ms) for otherwise non-hypergolic paraffin-based fuel. Thermochemical simulations reveal that the herein explored hypergolic MOFs could potentially closely match the theoretical specific impulse values of currently used hybrid rocket additives. The values, calculated for paraffin as the fuel matrix in combination with three popular different oxidizers (WFNA, LO_x and HTP), were compared to the performance achieved with currently used hypergolic (AB) and non-hypergolic fuel additives (aluminum). Although the calculated I_{sp} values were found to generally slightly decrease with the increase of the mass loading of HMOF in the paraffin fuel matrix, evaluating the change in I_{sp} as a function of oxidizer-to-fuel ratio revealed performance characteristics similar to those predicted for AB- and Al-containing fuel mixtures. The decrease in I_{sp} was found to be no more than 2.15% for a HMOF mass loading of 20 wt%. This minuscule decrease in performance is a very small cost for using a material that is much more thermally stable than AB as a means to enable hypergolicity within the rocket engine. Further studies will investigate the effect of the hypergolic MOF particle size on the ignition process and its implication on the range of additive mass loadings for which low ignition delays and reliable combustion can be achieved without a significant change in the regression rate of the paraffin fuel.

Data availability

An example of the hypergolic ignition may be found in the ESI.† Other videos of the experiments may be requested to the authors.

Author contributions

Olivier Jobin: conceptualization, investigation (ignition experiments, performance computations), writing – original draft. Cristina Mottillo: conceptualization, investigation (ignition experiments), writing – original draft. Hatem M. Titi: conceptualization, investigation (ignition experiments), writing – original draft. Joseph M. Marrett: investigation (HMOF preparation). Mihails Arhangelskis: investigation (periodic DFT calculation), writing – original draft. Robin D. Rogers: writing – review & editing. Bachar Elzein: writing – original draft. Tomislav Friščić: conceptualization, writing – review & editing. Étienne Robert: conceptualization, writing – review & editing.

Conflicts of interest

T. F., R. D. R., H. M. T., J. M. M. are inventors on patent application (no. 62/730,590, from 13 September 2018) related to hypergolic MOFs, which is assigned to ACSYNAM Inc. (Montreal, H1P 1W1, Canada) with T. F., C. M. and R. D. R. as co-owners.

Acknowledgements

Notes and references

1 G. Sutton and O. Biblarz, *Rocket Propulsion Elements*, John Wiley & Sons, 2010.

2 J. Malm, *Inclusion of Substances of Very High Concern in the Candidate List (Decision of the European Chemicals Agency), Document # ED/31/2011, European chemicals agency technical report*, 2011.

3 R. V. Petrescu, R. Aversa, B. Akash, R. Bucinell, J. Corchado, F. Berto, M. Mirsayar, A. Apicella, F. I. T. Petrescu, B. Akash, R. Bucinell, J. Corchado, A. Apicella and F. I. T. Petrescu, *Journal of Aircraft and Spacecraft Technology*, 2017, **1**, 1–8.

4 T. Harrison, A. Hunter, K. Johnson and T. Roberts, *Implication of Ultra-Low-Cost Access to Space*, Rowman & Littlefield, New York, USA, 2017.

5 R. W. Conversano, D. M. Goebel, R. R. Hofer, I. G. Mikellides and R. E. Wirz, *J. Propul. Power*, 2017, **33**, 975–983.

6 J. M. Bergthorson, Y. Yavor, J. Palecka, W. Georges, M. Soo, J. Vickery, S. Goroshin, D. L. Frost and A. J. Higgins, *Appl. Energy*, 2017, **186**, 13–27.

7 D. Ma, J. Murray and J. N. Munday, *Adv. Opt. Mater.*, 2017, **5**, 1600668.

8 National Aeronautics and Space Administration, *Reference Guide to The International Space Station*, 2015.

9 B. A. Palaszewski, M. L. Meyer, L. Johnson, D. M. Goebel, H. White and D. J. Coote, *Chemical Rocket Propulsion*, Springer, 2017, pp. 655–671.

10 M. C. Vilela Salgado, M. C. N. Belderrain and T. C. Devezas, *J. Aerosp. Technol. Manage.*, 2018, **10**, 1–23.

11 A. Mazzetti, L. Merotto and G. Pinarello, *Acta Astronaut.*, 2016, **126**, 286–297.

12 S. G. Kulkarni, V. S. Bagalkote, S. S. Patil, U. P. Kumar and V. A. Kumar, *Propellants, Explos., Pyrotech.*, 2009, **34**, 520–525.

13 L. He, G.-H. Tao, D. A. Parrish and J. M. Shreeve, *Chem.–Eur. J.*, 2010, **16**, 5736–5743.

14 M. Weismiller, T. Connell, G. Risha and R. Yetter, *46st AIAA/SAE/ASEE Joint Propulsion Conference*, Nashville, TN, 2010, pp. 1–12.

15 Y. Zhang, H. Gao, Y.-H. Joo and J. M. Shreeve, *Angew. Chem., Int. Ed.*, 2011, **50**, 9554–9562.

16 Y. Zhang and J. M. Shreeve, *Angew. Chem., Int. Ed.*, 2011, **50**, 935–937.

17 S. Schneider, T. Hawkins, Y. Ahmed, M. Rosander, L. Hudgens and J. Mills, *Angew. Chem., Int. Ed.*, 2011, **50**, 5886–5888.

18 P. V. Ramachandran, A. S. Kulkarni, M. A. Pfeil, J. D. Dennis, J. D. Willits, S. D. Heister, S. F. Son and T. L. Pourpoint, *Chem.–Eur. J.*, 2014, **20**, 16869–16872.

19 M. Pfeil, A. S. Kulkarni, P. V. Ramachandran, S. F. Son and S. D. Heister, *J. Propul. Power*, 2016, **32**, 23–31.

20 G. P. Rachiero, H. M. Titi and R. D. Rogers, *Chem. Commun.*, 2017, **53**, 7736–7739.

21 J. Yu, T. N. Jensen, W. K. Lewis, C. E. Bunker, S. P. Kelley, R. D. Rogers, O. M. Pryor, S. D. Chambreau, G. L. Vaghjiani and S. L. Anderson, *Energy Fuels*, 2018, **32**, 7898–7908.

22 A. K. Chinnam, N. Petrutik, K. Wang, A. Shlomovich, O. Shamis, D. S. Tov, M. Sućeska, Q.-L. Yan, R. Dobrovetsky and M. Gozin, *J. Mater. Chem. A*, 2018, **6**, 19989–19997.

23 K. Wang, A. K. Chinnam, N. Petrutik, E. P. Komarala, Q. Zhang, Q.-L. Yan, R. Dobrovetsky and M. Gozin, *J. Mater. Chem. A*, 2018, **6**, 22819–22829.

24 H. M. Titi, M. Arhangelskis, G. P. Rachiero, T. Friščić and R. D. Rogers, *Angew. Chem., Int. Ed.*, 2019, **58**, 18399–18404.

25 V. K. Bhosale, J. Jeong and S. Kwon, *Fuel*, 2019, **255**, 115729.

26 K. Wang, T. Liu, Y. Jin, S. Huang, N. Petrutik, D. Shem-Tov, Q.-L. Yan, M. Gozin and Q. Zhang, *J. Mater. Chem. A*, 2020, **8**, 14661–14670.

27 Q.-Y. Wang, J. Wang, S. Wang, Z.-Y. Wang, M. Cao, C.-L. He, J.-Q. Yang, S.-Q. Zang and T. C. W. Mak, *J. Am. Chem. Soc.*, 2020, **142**, 12010–12014.

28 L. Liang, Y. Zhong, Y. Xu, G. Lei, J. Chen, H. Huang, Z. Li, J. Zhang and T. Zhang, *Chem. Eng. J.*, 2021, **426**, 131866.

29 J. Jeong, V. K. Bhosale and S. Kwon, *Fuel*, 2021, **286**, 119307.

30 R. Masse, M. Allen, R. Spores and E. A. Driscoll, *52nd AIAA/SAE/ASEE Joint Propulsion Conference*, Salt Like City, UT, 2016, pp. 1–10.

31 R. Amrousse, T. Katsumi, N. Azuma and K. Hori, *Combust. Flame*, 2017, **176**, 334–348.

32 A. Karabeyoglu and U. Arkun, *50th AIAA/ASME/SAE/ASEE Joint Propulsion Conference*, Cleveland, OH, 2014, pp. 1–41.

33 M. Pfeil, PhD thesis, Purdue University, 2014.

34 B. Elzein, O. Jobin and E. Robert, *J. Propul. Power*, 2021, **37**, 77–85.

35 H.-C. J. Zhou and S. Kitagawa, *Chem. Soc. Rev.*, 2014, **43**, 5415–5418.

36 H.-C. Zhou, J. R. Long and O. M. Yaghi, *Chem. Rev.*, 2012, **112**, 673–674.

37 S. L. James, *Chem. Soc. Rev.*, 2003, **32**, 276.

38 Y. Cui, B. Li, H. He, W. Zhou, B. Chen and G. Qian, *Acc. Chem. Res.*, 2016, **49**, 483–493.

39 H. M. Titi, M. Arhangelskis, A. D. Katsenis, C. Mottillo, G. Ayoub, J.-L. Do, A. M. Fidelli, R. D. Rogers and T. Friščić, *Chem. Mater.*, 2019, **31**, 4882–4888.

40 H. M. Titi, J. M. Marrett, G. Dayaker, M. Arhangelskis, C. Mottillo, A. J. Morris, G. P. Rachiero, T. Friščić and R. D. Rogers, *Sci. Adv.*, 2019, **5**, 1–8.

41 J. T. Hughes, T. D. Bennett, A. K. Cheetham and A. Navrotsky, *J. Am. Chem. Soc.*, 2013, **135**, 598–601.

42 F. Baitalow, J. Baumann, G. Wolf, K. Jaenicke-Rößler and G. Leitner, *Thermochim. Acta*, 2002, **391**, 159–168.

43 B. Evans, N. Favorito, G. Risha, E. Boyer, R. Wehrman and K. Kuo, *40th AIAA/ASME/SAE/ASEE Joint Propulsion Conference and Exhibit*, Fort Lauderdale, FL, 2012, pp. 1–12.

44 S. Li, H. Gao and J. M. Shreeve, *Angew. Chem., Int. Ed.*, 2014, **53**, 2969–2972.

45 C. Wang, Y.-J. Wang, C.-L. He, Q.-Y. Wang and S.-Q. Zang, *JACS Au*, 2021, 1–6.

46 M. Barrere, A. Jaumotte, B. Fraeijis de Veubeke and J. Vandenkerckhove, *Rocket Propulsion (Propulsion de la fusée)*, Elsevier, 1960.

47 K. J. Stober, B. J. Cantwell and R. A. L. Otaibi, *J. Propul. Power*, 2020, **36**, 1–11.

48 S. J. Clark, M. D. Segall, C. J. Pickard, P. J. Hasnip, M. I. J. Probert, K. Refson and M. C. Payne, *Z. Kristallogr. - Cryst. Mater.*, 2005, **220**, 567–570.

49 T. Björkman, *Comput. Phys. Commun.*, 2011, **182**, 1183–1186.

50 K. Burke, J. P. Perdew and M. Ernzerhof, *Int. J. Quantum Chem.*, 1997, **61**, 287–293.

51 S. Grimme, *J. Comput. Chem.*, 2006, **27**, 1787–1799.

52 S. Gordon and B. J. Mcbride, *NASA RP-1311*, 1994.